ARTICLES

Spectra, energy levels, and transition line strengths for Sm^{3+}:$Y_3Al_5O_{12}$

John B. Gruber
Department of Physics, San Jose State University, San Jose, California 95192-0106

Bahram Zandi
Army Research Laboratory, Sensors and Electron Devices Directorate, 2800 Powder Mill Road, Adelphi, Maryland 20783-1197

Michael F. Reid
Department of Physics and Astronomy, University of Canterbury, Christchurch, New Zealand
(Received 29 January 1999)

Optical spectra and energy levels of the sextet, quartet, and doublet states of Sm^{3+} ($4f^5$) incorporated into single crystals of $Y_3Al_5O_{12}$ (Sm^{3+}:YAG), where YAG denotes yttrium aluminum garnet, are reported and analyzed at wavelengths between 560 and 280 nm. The analysis of energy (Stark) levels is based on a model Hamiltonian consisting of Coulombic, spin-orbit, and interconfigurational terms for the $4f^5$ atomic configuration of Sm^{3+} and crystal-field terms in D_2 symmetry (the site symmetry of the Sm^{3+} ions in the garnet lattice). The Hamiltonian also includes contributions arising from the spin-correlated crystal field. Because of the strength of the crystal field, the entire energy matrix is diagonalized within the complete $4f^5$ $SLJM_J$ basis set representing 73 *LS* states, 198 $^{2S+1}L_J$ multiplets, and 1001 doubly degenerate crystal-quantum states. In D_2 symmetry, all Stark levels are characterized by the same irreducible representation ($^2\Gamma_5$). Optimization between 314 calculated-to-observed Stark levels was carried out with a final rms deviation of 10 cm^{-1}. Eigenvectors obtained from the crystal-field splitting analysis are used to calculate transition line strengths originating from the ground-state Stark level to Stark levels in excited manifolds. The calculated line strengths are compared with experimental line strengths obtained from the absorption spectrum at 3.8 K. The line-strength analysis is useful in identifying individual excited Stark levels associated with sextet, quartet, and doublet states strongly mixed by the crystal field. [S0163-1829(99)09347-9]

I. INTRODUCTION

The crystal-field splitting of multiplet manifolds ^6H_J and ^6F_J of Sm^{3+} ($4f^5$) as a dopant in yttrium aluminum garnet, $Y_3Al_5O_{12}$ (YAG), has been analyzed by several groups.[1–3] These multiplets are the lowest in energy of 198 $^{2S+1}L_J$ multiplets associated with the $4f^5$ electronic configuration of Sm^{3+}. The most recent study assessed the potential for stimulated emission from $^4G(4)_{5/2}$ to individual energy (Stark) levels within the ^6H_J multiplet manifolds.[2] Stimulated emission involving Sm^{3+} has been reported at 618 nm (Sm^{3+}: glass).[4] In spite of its relatively weak transition line strengths, Sm^{3+} may be of interest as a visible laser ion, at least in the fiber geometry.

The visible and ultraviolet spectra of Sm^{3+} ($4f^5$) consist of transitions to numerous excited multiplet manifolds associated with the doublet, quartet, and sextet states of $4f^5$. We report an analysis of individual Stark levels and line strengths representing transitions from the ground-state Stark level in $^6H_{5/2}$ to excited-state Stark levels observed in the absorption spectrum obtained at 3.8 K between 560 and 280 nm. The spectrum consists of 314 transitions to 336 predicted Stark levels spanning 42 excited doublet, quartet, and sextet state multiplet manifolds between $^4G(4)_{5/2}$ (17 600 cm^{-1}) and $^2P(4)_{1/2}$ (35 550 cm^{-1}). The temperature-dependent (hot band) spectra obtained at 80 and 300 K establish the excited Stark levels of $^6H_{5/2}$ at 145 and 247 cm^{-1}. The site symmetry of Sm^{3+} in YAG is D_2 based on site-selective polarized spectroscopy of oriented crystals.[1,5] The symmetry is consistent with the assumption made in the past that the rare-earth ion (R^{3+}) substitutes for the Y^{3+} ions in D_2 symmetry sites in the lattice.[5,6]

Spectra representing transitions to many of the excited Stark levels are sufficiently resolved to make a quantitative determination of individual transition line strengths. The experimental levels and line strengths chosen for analysis are denoted by a footnote in Table I. Criteria for measuring line strengths are based on spectral separation between peaks having small or unchanging baselines, and a linewidth that can be measured reliably for a peak with an absorbance of 0.03 or higher. Eigenvectors obtained from the energy-level analysis were used to calculate the transition line strengths, which were then compared with experimental values obtained from the absorption spectrum at 3.8 K. Such an analysis helps to differentiate between transitions to excited doublet, quartet, and sextet states in the absorption spectrum.

The energy-level calculations are based on a model Hamiltonian that consists of Coulombic, spin-orbit, and interconfigurational terms for the $4f^5$ atomic configuration of Sm^{3+} and crystal-field terms in D_2 symmetry, including

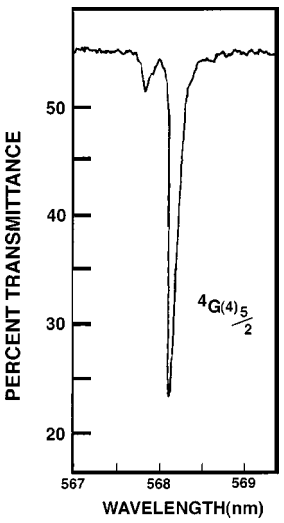

FIG. 1. Absorption spectrum of the lowest-energy Stark level of the $^4G(4)_{5/2}$ manifold obtained at 3.8 K showing satellite structure.

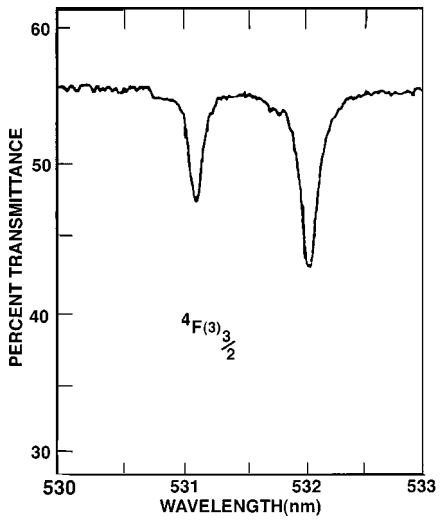

FIG. 2. Absorption spectrum of the $^4F(3)_{3/2}$ manifold obtained at 3.8 K.

spin-correlated crystal-field (CCF) contributions.[7,8] Because of the size of the crystal-field splitting, the total Hamiltonian was diagonalized within the complete $4f^5$ $SLJM_J$ basis set representing 73 LS states, 198 $^{2S+1}L_J$ multiplets, and 1001 doubly degenerate crystal-quantum states. A single matrix is required to diagonalize all Stark levels simultaneously, since all Stark levels belong to the same irreducible representation. From the spectroscopic analysis of energy levels and line strengths we obtain a detailed description of the complex mixing of doublet, quartet, and sextet states by the crystal field.

II. SPECTROSCOPIC MEASUREMENTS

Absorption spectra were obtained between 560 and 280 nm with a Cary Model 2390 spectrophotometer by Gruber and Hills on a crystal of Sm^{3+}:YAG obtained from Kokta.[9,10] Spectra at wavelengths shorter than 280 nm were not sufficiently resolved to merit an analysis of the detailed crystal-field splitting. A spectral bandwidth of about 0.05 nm was used where sharp peaks were observed having less than a 0.1-nm bandwidth at half-maximum. Calibration tests on the instrument indicated that the wavelength accuracy was better than 0.1 nm.

The absorption spectrum obtained at 3.8 K is given in Table I. The wavelengths (nm), the absorbances, and the energies (cm^{-1}) are given in the first three columns. The experimental line strengths are given in column 6. The Sm^{3+} ion concentration and the sample path length are reported in footnotes to Table I. The units of line strength are given in Debye units squared, where one Debye unit equals 10^{-18} esu or 3.36×10^{-30} C m. The observed line strengths in column 6 are weaker than the line strengths reported for the absorption spectra of the ^6H_J and ^6F_J multiplet manifolds.[1,2] This is not surprising given the fact that the visible and ultraviolet spectra primarily represent transitions to the quartet and doublet states of trivalent samarium. The most intense spectra appearing in Table I are found at wavelengths 419, 417, 405, 378, 365, and 348 nm. They are identified through an analysis of calculated-to-experimental energy levels and line strengths as having $^6P_J, M_J$ as the largest component in the wave function describing the state.

Emission spectra from the $^4G(4)_{5/2}$ to the ^6H_J and ^6F_J multiplet manifolds reported earlier[1,2] support the observation that a few Sm^{3+} ions are found in so-called ''minority'' sites. These sites are due to local site-symmetry modifications arising from impurities or defects that usually develop during crystal growth.[11–13] In Fig. 1 we show the absorption spectrum of the $^4G(4)_{5/2}$ observed at 3.8 K. Surrounding the strong central absorption peak, very weak structure is observed and is attributed to Sm^{3+} ions in minority sites.[12] We have chosen for line-strength analysis only the central peak that represents more than 90% of the total absorbance of the group. Less than 5% of all absorption peaks investigated show evidence of satellite structure.

The absorption spectrum appearing in Table I is not discernable as falling into groups that can be analyzed easily as the $J+\frac{1}{2}$ Stark components of an isolated multiplet. Exceptions can be found, however, such as $^4G(4)_{5/2}$ observed at 560 nm (Fig. 1) and $^4F(3)_{3/2}$ observed at 532 nm (Fig. 2). Two other examples include Fig. 3, the 3.8 K absorption spectrum of $^4G(4)_{7/2}$, and Fig. 4, the 3.8 K absorption spectrum of $^4P(2)_{5/2}$. The crystal field mixes the quartet, doublet, and ^6P states so thoroughly that a manifold centroid no longer has meaning in describing a single multiplet. Rajnak *et al.*[14] also found strong J mixing for similar states of Sm^{3+} in $LaCl_3$. An analysis of the calculated-to-experimental energy levels for Sm^{3+} in YAG requires the diagonalization of the complete energy matrix representing all sextet, quartet, and doublet states of the $4f^5$ electronic configuration.

III. THE MODEL HAMILTONIAN

The complete energy-level structure is analyzed in terms of a model Hamiltonian that assumes the Sm^{3+} ions occupy sites of D_2 symmetry in the lattice.[15] The Hamiltonian also includes interconfigurational mixing with other higher-energy configurations of like parity in the form of adjustable parameters, which for the most part remain reasonably fixed when Sm^{3+} energy levels are analyzed in different host materials.

The total Hamiltonian is expressed as follows:

TABLE I. Visible and ultraviolet spectra, energy levels, and line strengths in Sm^{3+}:YAG.

λ (nm)[a]	I[b]	E (cm^{-1})$_{obs}$[c]	E (cm^{-1})$_{calc}$[d]	ΔE (cm^{-1})[e]	S_{obs}[f]	S_{calc}[g]	$^{2S+1}L_J$[h]	M_J[i]	%	Level[j]
568.12	0.38	17597[k]	17599	2	700[l]	682	$^4G(4)_{5/2}$	±1/2	51%	55
559.31	0.06	17874[k]	17876	2	410[l]	611	$^4G(4)_{3/2}$	±3/2	71%	56
553.10	0.03	18076[k]	18071	−5	190[l]	142	$^4G(4)_{5/2}$	±5/2	57%	57
532.08	0.11	18789[k]	18809	20	620[l]	815	$^4F(3)_{3/2}$	±3/2	73%	58
531.16	0.05	18821[k]	18829	8	350[l]	340	$^4F(3)_{3/2}$	±1/2	75%	59
504.32	0.33	19823[k]	19798	−25	1560[l]	2629	$^4G(4)_{7/2}$	±3/2	52%	60
501.40	0.03	19934[k]	19931	−3	50[l]	54	$^4M_{15/2}$	±11/2	25%	61
501.20	0.51	19947[k]	19968	21	3120[l]	3310	$^4G(4)_{7/2}$	±5/2	53%	62
500.50	0.16	19967[k]	19987	20	710[l]	544	$^4G(4)_{7/2}$	±1/2	40%	63
499.5	0.17	20012[k]	20026	14	1220[l]	1859	$^4G(4)_{7/2}$	±1/2	17%	64
498.0	0.04	20075[k]	20081	6	320[l]	310	$^4G(4)_{7/2}$	±7/2	20%	65
495.65	0.04	20170[k]	20174	4	150[l]	155	$^4I(3)_{9/2}$	±1/2	28%	66
494.62	0.54	20212[k]	20230	18	2640[l]	2776	$^4M_{15/2}$	±15/2	21%	67
492.61	0.04	20295[k]	20292	−3	320[l]	343	$^4I(3)_{9/2}$	±7/2	40%	68
491.86	0.09	20325[k]	20330	5	670[l]	688	$^4I(3)_{9/2}$	±5/2	33%	69
489.78	0.11	20412[k]	20436	24	720[l]	682	$^4M_{15/2}$	±7/2	55%	70
487.5	0.03	20508	20516	8	150	159	$^4M_{15/2}$	±5/2	21%	71
486.5	0.06	20549[k]	20551	2	320[l]	310	$^4I(3)_{11/2}$	±9/2	15%	72
485.2	0.14	20604[k]	20595	−9	960[l]	1049	$^4I(3)_{11/2}$	±5/2	22%	73
483.8	0.07	20664[k]	20664	0	700[l]	651	$^4M_{15/2}$	±13/2	16%	74
483.2	0.21	20690[k]	20693	3	1785[l]	1726	$^4M_{15/2}$	±9/2	16%	75
481.8	0.05	20750[k]	20749	−1	250[l]	280	$^4I(3)_{9/2}$	±1/2	17%	76
481.0	0.10	20784[k]	20784	0	520[l]	640	$^4M_{15/2}$	±11/2	19%	77
479.4	0.36	20854[k]	20878	24	1020[l]	1174	$^4I(3)_{11/2}$	±3/2	33%	78
478.1	0.05	20910[k]	20910	0	850[l]	1425	$^4I(3)_{11/2}$	±9/2	26%	79
476.23	0.06	20992[k]	20974	−18	225[l]	387	$^4I(3)_{11/2}$	±11/2	38%	80
470.67	0.04	21240[k]	21239	−1	410[l]	565	$^4I(3)_{13/2}$	±3/2	22%	81
469.90	0.46	21275[k]	21278	3	1100[l]	1125	$^4I(3)_{13/2}$	±7/2	23%	82
469.6	0.03	21289[k]	21297	8	420[l]	551	$^4I(3)_{13/2}$	±3/2	34%	83
467.76	0.05	21372[k]	21362	−10	350[l]	329	$^4I(3)_{13/2}$	±13/2	42%	84
466.90	0.14	21411[k]	21384	−27	950[l]	1201	$^4I(3)_{13/2}$	±5/2	38%	85
465.75	0.24	21465[k]	21446	−19	1020[l]	1050	$^4I(3)_{13/2}$	±1/2	35%	86
464.8	0.25	21510[k]	21499	−11	1100[l]	1100	$^4I(3)_{13/2}$	±7/2	23%	87
464.35	0.34	21530[k]	21535	5	970[l]	1091	$^4I(3)_{13/2}$	±11/2	14%	88
462.98	0.10	21593[k]	21579	−14	520[l]	470	$^4I(3)_{13/2}$	±9/2	24%	89
455.8	0.10	21933[k]	21930	−3	530[l]	640	$^4F(3)_{5/2}$	±5/2	34%	90
454.8	0.12	21980[k]	21969	−13	590[l]	470	$^4F(3)_{5/2}$	±3/2	50%	91
453.7	0.08	22035[k]	22053	18	160[l]	81	$^4M_{17/2}$	±13/2	33%	92
452.8	0.08	22082[k]	22078	−2	260[l]	971	$^4M_{17/2}$	±15/2	18%	93
451.9	0.04	22123[k]	22122	−1	200[l]	240	$^4M_{17/2}$	±15/2	21%	94
451.63	0.03	22136[k]	22133	−3	120[l]	242	$^4M_{17/2}$	±7/2	37%	95
451.35	0.05	22150[k]	22152	2	200[l]	231	$^4M_{17/2}$	±9/2	21%	96
449.9	0.24	22221[k]	22204	−17	2520[l]	2460	$^4M_{17/2}$	±5/2	31%	97
448.08	0.05	22311[k]	22322	11	825[l]	972	$^4M_{17/2}$	±3/2	21%	98
444.47	0.15	22492[k]	22482	−10	430[l]	227	$^4M_{17/2}$	±13/2	18%	99
443.5	0.10	22544[k]	22544	0	410[l]	498	$^4G(4)_{9/2}$	±7/2	23%	100
442.1	0.04	22613[k]	22630	17	125[l]	130	$^4I(3)_{15/2}$	±15/2	10%	101
441.7	0.03	22632	22642	10	140	180	$^4I(3)_{15/2}$	±15/2	25%	102
440.75	0.05	22682[k]	22693	11	130[l]	112	$^4I(3)_{15/2}$	±9/2	24%	103
440.2	0.03	22711	22717	6	60	50	$^4I(3)_{15/2}$	±9/2	13%	104
439.42	0.04	22751[k]	22764	13	80[l]	72	$^4G(4)_{9/2}$	±3/2	26%	105
438.8	0.12	22783[k]	22776	−7	1285[l]	1379	$^4I(3)_{15/2}$	±7/2	23%	106
438.0	0.03	22823	22834	11	400	320	$^4I(3)_{15/2}$	±7/2	30%	107
437.65	0.03	22843[k]	22843	0	400	159	$^4G(4)_{9/2}$	±3/2	25%	108
437.35	0.03	22860	22854	−6	125	680	$^4G(4)_{9/2}$	±5/2	35%	109

TABLE I. (*Continued*).

λ (nm)[a]	I[b]	E (cm^{-1})$_{obs}$[c]	E (cm^{-1})$_{calc}$[d]	ΔE (cm^{-1})[e]	S_{obs}[f]	S_{calc}[g]	$^{2S+1}L_J$[h]	M_J[i]	%	Level[j]
436.2	0.04	22918[k]	22930	12	714[l]	700	$^4G(4)_{9/2}$	±9/2	35%	110
435.3	0.04	22963[k]	22965	2	720[l]	711	$^4G(4)_{9/2}$	±9/2	14%	111
434.7	0.02	22996	22983	−13		160	$^4I(3)_{15/2}$	±1/2	35%	112
434.0	0.02	23036	23034	−2		111	$^4I(3)_{15/2}$	±13/2	25%	113
433.75	0.03	23048	23043	−5	185	162	$^4I(3)_{15/2}$	±11/2	33%	114
425.06	0.04	23520[k]	23512	−8	225[l]	165	$^4M_{19/2}$	±15/2	38%	115
423.87	0.04	23586[k]	23583	−3	150[l]	150	$^4M_{19/2}$	±13/2	29%	116
422.06	0.02	23687	23681	−6		15	$^4M_{19/2}$	±1/2	21%	117
421.3	0.16	23730[k]	23728	−2	590[l]	414	$^4M_{19/2}$	±19/2	30%	118
420.96	0.18	23749[k]	23752	3	620[l]	62	$^4M_{19/2}$	±9/2	34%	119
420.19	0.39	23793[k]	23803	10	956[l]	922	$^4M_{19/2}$	±5/2	23%	120
419.50	1.03	23831[k]	23823	−8	4200[l]	4260	$^6P_{5/2}$	±1/2	40%	121
418.96	0.65	23862[k]	23863	1	2400[l]	2333	$^6P_{5/2}$	±3/2	68%	122
418.62	0.63	23882[k]	23881	−1	2480[l]	2183	$^4M_{19/2}$	±3/2	38%	123
418.25	0.50	23902[k]	23917	15	2220[l]	5173	$^4M_{19/2}$	±1/2	38%	124
417.37	1.20	23953[k]	23943	−10	7820[l]	7767	$^6P_{5/2}$	±5/2	45%	125
417.15	0.70	23965[k]	23973	8	2820[l]	2776	$^6P_{5/2}$	±5/2	20%	126
416.56	0.29	24000[k]	23983	−17	1000[l]	1040	$^4M_{19/2}$	±11/2	19%	127
412.70	0.08	24224[k]	24244	20	720[l]	644	$^4L_{13/2}$	±3/2	28%	128
412.17	0.08	24255[k]	24256	1	720[l]	732	$^4L_{13/2}$	±9/2	37%	129
411.42	0.08	24300[k]	24287	−13	720[l]	287	$^4L_{13/2}$	±11/2	29%	130
411.16	0.05	24315	24307	−8	514	354	$^4L_{13/2}$	±13/2	51%	131
409.5	0.15	24413[k]	24436	23	1620[l]	1852	$^4L_{13/2}$	±3/2	26%	132
408.2	0.03	24493	24488	−5	200	255	$^4L_{13/2}$	±11/2	30%	133
407.03	0.32	24562[k]	24549	−13	620[l]	657	$^4L_{13/2}$	±5/2	29%	134
405.52	1.67	24654[k]	24643	−11	33350[l]	30020	$^4M_{21/2}$	±21/2	49%	135
405.0	1.50	24686[k]	24690	4	22000[l]	23363	$^6P_{3/2}$	±3/2	49%	136
404.6	2.00	24709[k]	24714	5	40000[l]	40370	$^6P_{3/2}$	±1/2	40%	137
404.1	1.78	24740[k]	24739	−1	28700[l]	28751	$^6P_{3/2}$	±1/2	46%	138
403.69	1.01	24765[k]	24759	−6	22050[l]	21893	$^4F(3)_{7/2}$	±5/2	25%	139
403.42	1.00	24781[k]	24793	12	21580[l]	21645	$^4F(3)_{7/2}$	±3/2	30%	140
402.71	0.13	24825[k]	24820	−5	1675[l]	1334	$^4M_{21/2}$	±11/2	30%	141
402.37	0.05	24846[k]	24835	−11	290[l]	275	$^4M_{21/2}$	±13/2	17%	142
401.8	0.03	24880[k]	24877	−3	120	363	$^4K(1)_{11/2}$	±5/2	28%	143
401.46	0.03	24900[k]	24896	−4	100[l]	49	$^4K(1)_{11/2}$	±3/2	52%	144
400.7	0.03	24946[k]	24943	−3	100	103	$^4K(1)_{11/2}$	±5/2	24%	145
400.65	0.06	24952[k]	24957	5	250[l]	230	$^4M_{21/2}$	±9/2	16%	146
400.34	0.03	24972[k]	24969	−3	85	12	$^4M_{21/2}$	±11/2	25%	147
399.73	0.04	25010[k]	25012	2	185[l]	43	$^4M_{21/2}$	±9/2	20%	148
399.3	0.06	25036[k]	25029	−7	120[l]	36	$^4M_{21/2}$	±5/2	20%	149
398.8	0.06	25070[k]	25082	12	250[l]	196	$^4K(1)_{11/2}$	±1/2	14%	150
398.6	0.04	25085[k]	25096	11	210	52	$^4K(1)_{11/2}$	±7/2	23%	151
397.98	0.03	25120[k]	25130	10	320	411	$^4K(1)_{11/2}$	±9/2	32%	152
397.04	0.03	25179[k]	25164	−15	250	210	$^4L_{15/2}$	±7/2	15%	153
395.32	0.08	25289[k]	25289	0	820[l]	835	$^4L_{15/2}$	±5/2	31%	154
395.3	0.06	25293[k]	25291	−2	1000[l]	971	$^4L_{15/2}$	±3/2	34%	155
395.0	0.02	25310	25308	−2		120	$^4L_{15/2}$	±7/2	23%	156
394.67	0.04	25330[k]	25333	3	250[l]	258	$^4L_{15/2}$	±9/2	28%	157
393.87	0.03	25382[k]	25381	−1	200	238	$^4L_{15/2}$	±15/2	38%	158
393.82	0.17	25385[k]	25383	−2	520[l]	382	$^4M_{21/2}$	±3/2	31%	159
392.90	0.20	25445[k]	25433	−12	625[l]	482	$^4M_{21/2}$	±1/2	33%	160
392.43	0.30	25475[k]	25501	26	825[l]	502	$^4G(4)_{11/2}$	±1/2	14%	161
391.90	0.06	25510[k]	25530	20	250	68	$^4M_{21/2}$	±17/2	27%	162
391.13	0.06	25560[k]	25550	−10	225	95	$^4M_{21/2}$	±19/2	29%	163
390.68	0.14	25589[k]	25582	−7	1425[l]	1333	$^4G(4)_{11/2}$	±1/2	39%	164

TABLE I. (*Continued*).

λ (nm)[a]	I[b]	E (cm^{-1})$_{obs}$[c]	E (cm^{-1})$_{calc}$[d]	ΔE (cm^{-1})[e]	S_{obs}[f]	S_{calc}[g]	$^{2S+1}L_J$[h]	M_J[i]	%	Level[j]
390.4	0.08	25610[k]	25603	−7	300[l]	333	$^4G(4)_{11/2}$	±7/2	17%	165
390.1	0.16	25630[k]	25622	−8	1600[l]	1586	$^4G(4)_{11/2}$	±9/2	54%	166
389.85	0.16	25645[k]	25649	4	750[l]	793	$^4L_{15/2}$	±13/2	29%	167
389.69	0.16	25654[k]	25652	−2	760[l]	738	$^4L_{15/2}$	±1/2	20%	168
388.85	0.10	25710[k]	25715	5	725[l]	663	$^4G(4)_{11/2}$	±7/2	26%	169
388.24	0.06	25750[k]	25748	−2	540[l]	252	$^4G(4)_{11/2}$	±11/2	39%	170
387.7	0.03	25786[k]	25785	−1	320	240	$^4G(4)_{11/2}$	±5/2	48%	171
380.05	0.20	26305[k]	26306	1	1810[l]	2000	$^4D(3)_{1/2}$	±1/2	44%	172
379.69	0.03	26330[k]	26320	−10	425	342	$^4L_{17/2}$	±5/2	30%	173
379.45	0.04	26347[k]	26339	−8	520[l]	417	$^4L_{17/2}$	±9/2	30%	174
378.90	0.62	26385[k]	26366	−19	2643[l]	2164	$^4D(3)_{1/2}$	±1/2	24%	175
378.68	0.05	26400[k]	26395	15	252	570	$^4L_{17/2}$	±7/2	17%	176
378.52	0.05	26412[k]	26410	−2	550[l]	693	$^4L_{17/2}$	±9/2	23%	177
377.98	0.87	26449[k]	26465	16	3700[l]	3710	$^6P_{7/2}$	±7/2	32%	178
377.8	0.24	26456[k]	26469	13	1280[l]	1295	$^4L_{17/2}$	±17/2	38%	179
377.19	1.00	26504[k]	26497	−7	13100[l]	13056	$^6P_{7/2}$	±5/2	40%	180
377.05	0.20	26514[k]	26513	−1	6425[l]	6690	$^6P_{7/2}$	±3/2	34%	181
376.74	1.10	26536[k]	26536	0	27000[l]	27160	$^6P_{7/2}$	±1/2	53%	182
376.2	0.57	26578[k]	26585	7	11946[l]	11768	$^6P_{7/2}$	±3/2	25%	183
375.58	0.39	26618[k]	26634	16	1025[l]	466	$^4K(1)_{13/2}$	±5/2	30%	184
375.24	0.11	26642[k]	26656	14	360[l]	186	$^4K(1)_{13/2}$	±7/2	25%	185
374.82	0.05	26672[k]	26672	0	225[l]	200	$^4K(1)_{13/2}$	±3/2	40%	186
374.56	0.02	26690	26687	−3		40	$^4K(1)_{13/2}$	±7/2	16%	187
373.90	0.06	26738[k]	26739	1	725[l]	126	$^4K(1)_{13/2}$	±9/2	30%	188
373.44	0.02	26770	26756	−14	100	191	$^4K(1)_{13/2}$	±1/2	15%	189
372.77	0.16	26819[k]	26822	3	1025[l]	995	$^4K(1)_{13/2}$	±1/2	20%	190
371.5	0.02	26914[k]	26921	7		150	$^4K(1)_{13/2}$	±11/2	46%	191
370.54	0.03	26980[k]	26970	−10	180	160	$^4K(1)_{13/2}$	±13/2	17%	192
368.22	0.02	27150[k]	27152	2		140	$^4F(3)_{9/2}$	±5/2	33%	193
367.55	0.11	27200[k]	27205	5	1185[l]	1205	$^4F(3)_{9/2}$	±3/2	44%	194
367.18	0.17	27227[k]	27235	8	3300[l]	3240	$^4D(2)_{3/2}$	±3/2	31%	195
365.94	0.25	27317[k]	27302	−15	5130[l]	4740	$^4F(3)_{9/2}$	±1/2	37%	196
365.40	0.20	27363[k]	27373	10	2420[l]	3456	$^6P_{5/2}$	±1/2	56%	197
364.37	0.14	27437[k]	27432	−5	1400[l]	720	$^6P_{5/2}$	±5/2	24%	198
363.7	0.44	27490[k]	27485	−5	5620[l]	5733	$^6P_{5/2}$	±3/2	38%	199
362.8	0.40	27555[k]	27559	4	2440	2331	$^4D(2)_{3/2}$	±1/2	33%	200
362.7	0.45	27559[k]	27565	6	14400[l]	14340	$^6P_{5/2}$	±5/2	43%	201
362.5	0.14	27578[k]	27574	−4	1490[l]	1574	$^4F(3)_{9/2}$	±5/2	18%	202
358.3	0.04	27902[k]	27896	−6	200	201	$^4H(1)_{7/2}$	±3/2	63%	203
356.86	0.05	28014[k]	27990	−24	250	74	$^4H(1)_{7/2}$	±5/2	38%	204
355.78	0.06	28100[k]	28089	−11	300[l]	306	$^4H(1)_{7/2}$	±7/2	51%	205
355.5	0.06	28120[k]	28108	−18	450	965	$^4H(1)_{7/2}$	±1/2	52%	206
352.2	0.03	28386[k]	28387	1	130[l]	133	$^4K(1)_{15/2}$	±1/2	50%	207
352.1	0.02	28390[k]	28398	8		36	$^4K(1)_{15/2}$	±3/2	44%	208
351.9	0.10	28410[k]	28416	6	520[l]	270	$^4K(1)_{15/2}$	±7/2	54%	209
351.63	0.06	28431[k]	28426	−5	210[l]	207	$^4K(1)_{15/2}$	±5/2	26%	210
351.4	0.25	28450[k]	28448	−2	1260[l]	350	$^4K(1)_{15/2}$	±5/2	26%	211
351.13	0.07	28470[k]	28469	−1	450[l]	184	$^4K(1)_{15/2}$	±15/2	64%	212
350.58	0.10	28516[k]	28511	−5	500[l]	270	$^4K(1)_{15/2}$	±11/2	26%	213
350.11	0.07	28554[k]	28551	−3	300[l]	350	$^4K(1)_{15/2}$	±13/2	52%	214
349.39	0.16	28613[k]	28604	−9	1150[l]	1133	$^6P_{7/2}$	±3/2	17%	215
348.98	0.05	28647[k]	28638	−9	500[l]	140	$^4H(1)_{9/2}$	±3/2	44%	216
348.8	0.26	28664[k]	28662	−2	560[l]	558	$^4H(1)_{9/2}$	±5/2	25%	217
348.69	0.10	28672[k]	28672	0	340	625	$^4H(1)_{9/2}$	±9/2	10%	218
348.47	0.40	28689[k]	28694	−5	3200[l]	3380	$^6P_{7/2}$	±5/2	18%	219

TABLE I. (*Continued*).

λ (nm)[a]	I[b]	E (cm^{-1})$_{obs}$[c]	E (cm^{-1})$_{calc}$[d]	ΔE (cm^{-1})[e]	S_{obs}[f]	S_{calc}[g]	$^{2S+1}L_J$[h]	M_J[i]	%	Level[j]
348.28	0.38	28704[k]	28705	1	3000[l]	3047	$^6P_{7/2}$	±1/2	18%	220
347.98	0.21	28729[k]	28739	10	4820[l]	4840	$^6P_{7/2}$	±1/2	14%	221
347.75	0.10	28748[k]	28746	−2	1900[l]	1902	$^6P_{7/2}$	±7/2	29%	222
347.43	0.32	28775[k]	28766	−9	4525[l]	4538	$^4K(1)_{17/2}$	±15/2	16%	223
347.27	0.17	28788[k]	28794	6	1120[l]	1125	$^4K(1)_{17/2}$	±1/2	21%	224
347.0	0.20	28810[k]	28811	1	1240[l]	1240	$^4K(1)_{17/2}$	±15/2	20%	225
346.91	0.98	28818[k]	28831	13	10000[l]	9776	$^6P_{7/2}$	±3/2	15%	226
346.64	0.14	28840[k]	28838	−2	740[l]	850	$^4K(1)_{17/2}$	±1/2	19%	227
346.48	1.00	28853[k]	28866	13	4840[l]	4107	$^4K(1)_{17/2}$	±17/2	18%	228
346.23	0.55	28866[k]	28877	11	1000[l]	923	$^4K(1)_{17/2}$	±17/2	15%	229
345.93	0.70	28900[k]	28895	−5	1320[l]	460	$^4K(1)_{17/2}$	±13/2	14%	230
345.68	0.27	28920[k]	28919	−1	140	320	$^4H(1)_{11/2}$	±5/2	23%	231
345.37	0.14	28946[k]	28932	−14	520	360	$^4H(1)_{11/2}$	±11/2	22%	232
345.2	0.47	28960[k]	28973	13	1625[l]	1860	$^6P_{7/2}$	±1/2	19%	233
344.93	0.11	28983[k]	28982	−1	620[l]	346	$^4H(1)_{11/2}$	±7/2	15%	234
344.6	0.05	29011[k]	29022	11	310	220	$^4L_{19/2}$	±13/2	14%	235
344.43	0.10	29025[k]	29024	−1	740[l]	106	$^4H(1)_{11/2}$	±9/2	15%	236
344.22	0.05	29043[k]	29048	5	300	216	$^4L_{19/2}$	±19/2	17%	237
344.0	0.03	29060[k]	29057	−3	260	340	$^4L_{19/2}$	±19/2	13%	238
343.9	0.03	29069[k]	29066	−3	240	120	$^4H(1)_{11/2}$	±1/2	24%	239
343.5	0.02	29104	29116	12		130	$^4L_{19/2}$	±3/2	12%	240
343.2	0.05	29129[k]	29127	−2	420[l]	676	$^4K(1)_{17/2}$	±5/2	12%	241
342.9	0.03	29155[k]	29163	8	320	183	$^4K(1)_{17/2}$	±9/2	16%	242
342.4	0.02	29197[k]	29191	−6		68	$^4L_{19/2}$	±17/2	28%	243
341.78	0.02	29250[k]	29247	−3		183	$^4L_{19/2}$	±17/2	13%	244
341.6	0.01	29266	29251	−15		47	$^4H(1)_{13/2}$	±3/2	24%	245
341.21	0.01	29299	29282	−17		42	$^4H(1)_{13/2}$	±5/2	35%	246
340.2	0.03	29386[k]	29388	2	85	67	$^4H(1)_{13/2}$	±7/2	24%	247
340.1	0.03	29395[k]	29392	−3	85	63	$^4H(1)_{13/2}$	±13/2	44%	248
339.7	0.03	29429	29430	1	85	122	$^4H(1)_{13/2}$	±3/2	36%	249
339.4	0.01	29455	29454	−1	50	15	$^4H(1)_{13/2}$	±9/2	26%	250
339.02	0.04	29488[k]	29488	0	325[l]	198	$^4H(1)_{13/2}$	±1/2	30%	251
338.9	0.03	29500[k]	29492	−8	310[l]	274	$^4L_{19/2}$	±1/2	16%	252
338.4	0.03	29542[k]	29540	−2	150	126	$^4H(1)_{13/2}$	±11/2	21%	253
338.29	0.02	29552[k]	29551	−1		134	$^4H(1)_{13/2}$	±11/2	26%	254
337.83	0.03	29592[k]	29584	−8	100	100	$^4L_{19/2}$	±15/2	31%	255
337.14	0.04	29653[k]	29653	0	325[l]	337	$^4G(2)_{7/2}$	±7/2	25%	256
335.47	0.03	29800	29793	−7	200	307	$^4G(2)_{7/2}$	±7/2	28%	257
335.08	0.02	29835	29839	4	200	228	$^4G(2)_{7/2}$	±3/2	55%	258
334.8	0.05	29860[k]	29864	4	420[l]	161	$^4G(2)_{9/2}$	±7/2	29%	259
334.58	0.16	29880[k]	29886	6	195	386	$^4G(2)_{7/2}$	±5/2	22%	260
334.15	0.08	29918[k]	29898	−20	420[l]	151	$^4G(2)_{5/2}$	±5/2	20%	261
333.68	0.02	29960[k]	29962	2		18	$^4G(2)_{7/2}$	±1/2	25%	262
333.24	0.01	30000	30014	14		133	$^4G(2)_{9/2}$	±1/2	26%	263
333.04	0.01	30018	30030	12		6	$^4G(2)_{9/2}$	±5/2	30%	264
331.98	0.06	30114[k]	30089	−25	225[l]	236	$^4G(2)_{5/2}$	±1/2	43%	265
330.2	0.04	30276[k]	30272	−4	150	55	$^4G(2)_{5/2}$	±5/2	31%	266
329.4	0.25	30350[k]	30347	−3	460[l]	193	$^4G(2)_{5/2}$	±1/2	37%	267
324.22	0.05	30834[k]	30838	4	200	111	$^2L(3)_{15/2}$	±15/2	43%	268
323.74	0.03	30880[k]	30884	4	50	100	$^2L(3)_{15/2}$	±1/2	29%	269
323.34	0.01	30918	30921	3		5	$^2L(3)_{15/2}$	±9/2	61%	270
322.12	0.02	31035[k]	31029	−6		45	$^2L(3)_{15/2}$	±7/2	51%	271
321.8	0.03	31066[k]	31089	23	150	161	$^4P(2)_{1/2}$	±1/2	77%	272
321.23	0.04	31121[k]	31122	1	260[l]	284	$^4G(2)_{11/2}$	±9/2	28%	273
320.94	0.04	31149[k]	31150	1	290[l]	329	$^4G(2)_{11/2}$	±9/2	40%	274
320.5	0.15	31192[k]	31191	−1	850[l]	724	$^3L(3)_{15/2}$	±5/2	20%	275
320.35	0.02	31207[k]	31207	0		72	$^4G(2)_{11/2}$	±7/2	31%	276
319.98	0.02	31243[k]	31242	−1		65	$^4G(2)_{11/2}$	±11/2	45%	277
319.83	0.35	31258[k]	31263	5	200[l]	155	$^2L(3)_{15/2}$	±13/2	20%	278
319.45	0.04	31295[k]	31309	14	1600[l]	1536	$^4G(2)_{11/2}$	±1/2	44%	279
319.12	0.04	31327[k]	31334	7	175	155	$^4G(2)_{11/2}$	±3/2	28%	280
317.74	0.07	31464[k]	31464	0	425[l]	156	$^2L(3)_{15/2}$	±1/2	20%	281
317.54	0.04	31483[k]	31475	−8	250	50	$^2L(3)_{15/1}$	±11/2	23%	282
316.8	0.19	31557[k]	31545	−12	1000[l]	935	$^4G(2)_{11/2}$	±7/2	37%	283
313.05	0.24	31631	31624	−7	1685[l]	1745	$^4P(2)_{3/2}$	±1/2	48%	284
307.07	0.07	32525[k]	32521	−14	175	185	$^4P(2)_{5/2}$	±1/2	45%	285
306.02	0.61	32594[k]	32586	−8	1675[l]	1825	$^4P(2)_{5/2}$	±3/2	56%	286

TABLE I. (*Continued*).

λ (nm)[a]	I[b]	E (cm^{-1})$_{obs}$[c]	E (cm^{-1})$_{calc}$[d]	ΔE (cm^{-1})[e]	S_{obs}[f]	S_{calc}[g]	$^{2S+1}L_J$[h]	M_J[i]	%	Level[j]
305.82	0.31	32647[k]	32630	−17	925[l]	972	$^4P(2)_{5/2}$	±1/2	44%	287
301.92	0.04	33112[k]	33102	−10	225	60	$^2F(5)_{5/2}$	±1/2	40%	288
301.2	0.04	33191[k]	33217	26	240	82	$^2K(5)_{13/2}$	±1/2	22%	289
300.75	0.02	33241	33261	20		34	$^2K(5)_{13/2}$	±13/2	29%	290
300.5	0.03	33268[k]	33268	0	100	64	$^2K(5)_{13/2}$	±9/2	24%	291
298.67	0.03	33472[k]	33471	−1	100	45	$^4F(2)_{5/2}$	±9/2	61%	292
298.42	0.10	33500[k]	33509	9	280[l]	265	$^2K(5)_{13/2}$	±3/2	22%	293
298.33	0.03	33510[k]	33524	14	90	24	$^2K(5)_{13/2}$	±3/2	22%	294
297.95	0.03	33553[k]	33566	13	90	66	$^4F(2)_{5/2}$	±7/2	42%	295
297.45	0.02	33609[k]	33604	−5		5	$^4F(2)_{5/2}$	±1/2	53%	296
297.15	0.02	33643[k]	33639	−4		11	$^4F(2)_{5/2}$	±7/2	29%	297
296.95	0.01	33666[k]	33656	−10		52	$^4F(2)_{5/2}$	±5/2	37%	298
296.8	0.01	33683[k]	33670	−13		34	$^2K(5)_{13/2}$	±11/2	25%	299
296.25	0.01	33745	33726	−19		9	$^2K(5)_{13/2}$	±11/2	35%	300
295.88	0.03	33788[k]	33779	−9	100	54	$^2F(5)_{5/2}$	±3/2	21%	301
295.25	0.03	33861[k]	33851	−10	70	37	$^2L(3)_{17/2}$	±9/2	24%	302
295.16	0.01	33870	33855	−15	63	81	$^2L(3)_{17/2}$	±17/2	22%	303
294.56	0.03	33939[k]	33929	−10	15	22	$^2L(3)_{17/2}$	±7/2	22%	304
294.58	0.01	33936	33932	−4		15	$^4I(2)_{9/2}$	±9/2	31%	305
294.2	0.01	33980	33974	−6		1	$^2L(3)_{17/2}$	±9/2	20%	306
294.18	0.02	33983[k]	33979	−4		37	$^2L(3)_{17/2}$	±11/2	34%	307
293.9	0.01	34015	34016	−1		5	$^2L(3)_{17/2}$	±9/2	22%	308
293.7	0.01	34038	34039	1		5	$^2L(3)_{17/2}$	±9/2	22%	309
293.3	0.03	34085[k]	34085	0	60[l]	89	$^4L(2)_{9/2}$	±3/2	29%	310
292.83	0.02	34140[k]	34144	4		17	$^2L(3)_{17/2}$	±13/2	27%	311
292.7	0.01	31455	34149	−6		3	$^2L(3)_{17/2}$	±3/2	40%	312
292.57	0.01	34170[k]	34170	0		2	$^2L(3)_{17/2}$	±15/2	58%	313
292.4	0.01	34190	34198	8		2	$^2L(3)_{17/2}$	±1/2	32%	314
291.71	0.04	34271[k]	34287	7	100	120	$^4I(2)_{9/2}$	±5/2	39%	315
291.5	0.04	34295[k]	34297	2	100	79	$^4I(2)_{9/2}$	±3/2	39%	316
285.63	0.01	35000[k]	35003	3		4	$^2N_{19/2}$	±17/2	86%	317
285.55	0.01	35010	35008	−2		3	$^2N_{19/2}$	±19/2	64%	318
284.65	0.01	35120[k]	35111	−9		10	$^2N_{19/2}$	±15/2	60%	319
284.5	0.01	35139	35151	12		4	$^2N_{19/2}$	±13/2	41%	320
284.27	0.01	35167[k]	35165	−2		31	$^2N_{19/2}$	±11/2	32%	321
284.1	0.01	35188	35182	−6		10	$^2N_{19/2}$	±9/2	42%	322
284.01	0.01	35200	35196	−4		13	$^2N_{19/2}$	±7/2	31%	323
283.87	0.06	35217[k]	35214	−3	165	103	$^4F(2)_{7/2}$	±3/2	34%	324
283.81	0.01	35225[k]	35221	−4		10	$^2N_{19/2}$	±1/2	21%	325
283.52	0.01	35260	35251	−9		4	$^2N_{19/2}$	±3/2	25%	326
283.48	0.06	35264[k]	35257	−7	170[l]	187	$^4F(2)_{7/2}$	±3/2	28%	327
283.36	0.03	35280[k]	35274	−6	23	35	$^4F(2)_{7/2}$	±7/2	18%	328
282.96	0.03	35330[k]	35333	3	23	59	$^4I(2)_{11/2}$	±11/2	44%	329
282.52	0.03	35385[k]	35391	6	49	85	$^4I(2)_{11/2}$	±9/2	47%	330
282.08	0.01	35440[k]	35432	−8		20	$^4F(2)_{7/2}$	±5/2	64%	331
281.93	0.01	35459	35454	−5		18	$^4F(2)_{7/2}$	±1/2	55%	332
281.8	0.02	35475[k]	35473	−2		59	$^4I(2)_{11/2}$	±1/2	34%	333
281.21	0.05	35550[k]	35558	8	170[l]	201	$^2P(4)_{1/2}$	±1/2	94%	334
281.1	0.10	35564[k]	35570	6	825[l]	1294	$^4I(2)_{11/2}$	±7/2	31%	335
280.66	0.03	35620[k]	35622	2	123	76	$^4I(2)_{11/2}$	±5/2	48%	336

[a]Wavelength in nanometers; spectrum obtained at sample temperature 3.8 K.

[b]Absorbance units; sample thickness, 0.35 cm; Sm^{3+} concentration, 3.4×10^{18} ions/cm^3.

[c]Experimental energy in vacuum wave numbers.

[d]Calculated energy in vacuum wave numbers using parameters reported in Table III col. 2.

[e]Difference in energy, $E_{calc}-E_{obs}$ in cm^{-1}.

[f]Observed transition line strength, $S_{1\rightarrow n}$ from level one to excited levels n, in units of 10^{-8} debye squared (D^2, Ref. 25); refractive index correction at wavelength of transition is also given in Ref. 25.

[g]Calculated absorption line strength in units of $10^{-8}D^2$ using parameters reported in Table IV, col. 3.

[h]Multiplet label for which the largest percent M_J contribution is given in footnote i.

[i]Largest percent M_J contribution to the wave function for the designated Stark level.

[j]Stark level beginning with the ground-state Stark level in $^6H_{5/2}$ as the first (1) level.

[k]Levels used in fitting calculated-to-observed energy levels.

[l]Levels selected for line strength analysis.

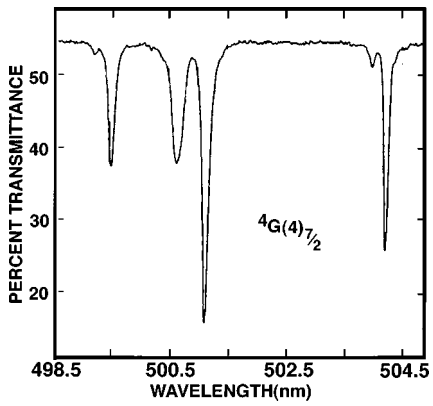

FIG. 3. Absorption spectrum of the $^4G(4)_{7/2}$ manifold obtained at 3.8 K.

$$\hat{H}=\hat{H}_a+\hat{H}_{\rm cf}+\hat{H}_{\rm ccf}, \tag{1}$$

where $\hat{H}_a$ represents the isotropic terms in the atomic Hamiltonian, including the spherically symmetric parts of the $4f$-electron crystal-field interactions, $\hat{H}_{\rm cf}$ represents the nonspherically symmetric terms of the one-electron crystal-field interactions, and $\hat{H}_{\rm ccf}$ incorporates two-electron correlation-crystal-field (ccf) interactions into the Hamiltonian.[7,8] The terms in $\hat{H}_a$ include,

$$\hat{H}_a=\langle E\rangle+\sum_k F^k\hat{f}_k+\alpha\hat{L}(\hat{L}+1)+\beta\hat{G}(G_2)+\gamma\hat{G}(R_7)$$

$$+\sum_i T^i\hat{t}_i+\zeta_{\rm s.o.}\hat{A}_{\rm s.o.}+\sum_k P^k\hat{p}_k+\sum_j M^j\hat{m}_j, \tag{2}$$

where $k=2,4,6$; $i=2,3,4,6,7,8$; $j=0,2,4$; and the operators $(\hat{o})$ and their associated parameters are expressed in conventional notation with respect to the interactions they represent.[15–18]

The one-electron crystal-field Hamiltonian is expressed as

$$\hat{H}_{\rm cf}=\sum_{k,q} B_q^k\hat{C}_q^{(k)}, \tag{3}$$

where $k=2,4,6$ (with $|q|\leqslant k$), $\hat{C}_q^{(k)}$ is an intraconfigurational spherical-tensor operator of rank k and order q, and the B_q^k represent one-electron crystal-field-splitting parameters with $B_{-q}^k=(-1)^qB_q^k$. In D_2 symmetry there are nine independent B_q^k parameters which we adjust to give the best overall agreement between the calculated and observed crystal-field splitting.[18]

The third term in Eq. (1) includes contributions attributable to differences in the crystal field as seen by $4f$ electrons with different spins relative to the direction of the total spin of the electrons in the configuration.[19–22] Called the correlation crystal field (ccf), its Hamiltonian is expressed as

$$\hat{H}_{\rm ccf}=\sum_{k,i,q} G_{iq}^k\hat{g}_{iq}^{(k)}, \tag{4}$$

where $k=0,2,4,6,8,10,12$. The sum over i distinguishes different operators and parameters with identical k, and $q=0$, $\pm2,\pm4,\pm6$, $|q|\leqslant k$. The G_{iq}^k terms are adjustable parameters.[8,20,21] When Eq. (4) is included in the total Hamiltonian given in Eq. (1), some of the interaction terms disappear as they are already represented in either Eq. (2) or Eq. (3). The Hamiltonian given in Eq. (1) was diagonalized within the complete $SLJM_J$ basis set of the $4f^5$ electronic configuration that includes 73 LS states, 198 $^{2S+1}L_J$ multiplets, and 1001 Stark levels. Since Sm^{3+} is a Kramers ion, each Stark level is twofold degenerate in sites of D_2 symmetry.

IV. ANALYSIS OF ENERGY LEVELS

To check the results obtained from the diagonalization of the complete energy matrix, we first calculated the splitting of the ^6H_J and ^6F_J multiplet manifolds using the final set of B_q^k parameters obtained from Ref. 2. The results were compared with the experimental Stark levels reported by Gruber *et al.*[1] listed as levels 1 through 54 in Table II. Level 55 represents the lowest-energy Stark level of $^4G(4)_{5/2}$ (17 597 cm^{-1}), which is the first entry in Table I. Without performing any least-squares fitting between the calculated and experimental levels, we obtain a rms deviation within the value quoted in Ref. 2.

The same B_q^k parameters were then used as a starting set to calculate the splitting of the multiplet manifolds appearing in Table I. The experimental levels given in Table II were also included in this fitting. We chose reasonably isolated multiplet manifolds between 17 600 and 25 000 cm^{-1} such as $^4G(4)_{5/2}$, $^4F(3)_{3/2}$, $^4G(4)_{7/2}$, $^4I(3)_{13/2}$, $^4M_{17/2}$, $^4I(3)_{15/2}$, $^4G(4)_{9/2}$, $^6P_{5/2}$, $^4L(4)_{13/2}$, and $^6P_{3/2}$ for a least-squares fitting between calculated-to-experimental Stark levels. This analysis was then extended to include reasonably isolated multiplet manifolds having energies up to 35 000 cm^{-1}.

Since the entire energy matrix is diagonalized with adjustable atomic and crystal-field parameters, we avoid arbitrary adjustment of multiplet manifold centers of gravity (centroids). Thus, we avoid the truncation errors present in earlier crystal-field-splitting calculations for Sm^{3+} in host crystals.[2,14] We are able to extend the analysis to numerous multiplets where the crystal-field mixing is so large that the

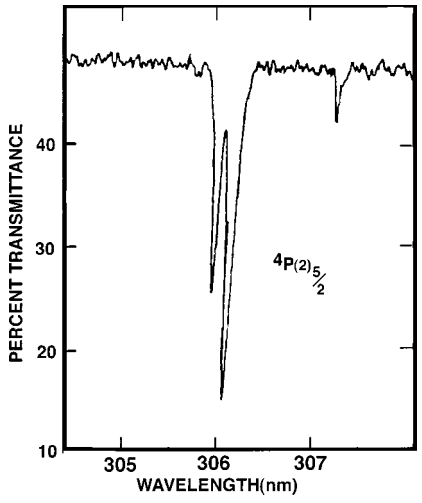

FIG. 4. Absorption spectrum of the $^4P(2)_{5/2}$ manifold obtained at 3.8 K.

TABLE II. Energy levels of the sextet states, ^6H_J and ^6F_J in Sm^{3+}:YAG.

Level[a]	E (cm^{-1})$_{obs}$[b]	E (cm^{-1})$_{calc}$[c]	$^{2S+1}L_J$[d]	M_J, %[e]		Level[a]	E (cm^{-1})$_{obs}$[b]	E (cm^{-1})$_{calc}$[c]	$^{2S+1}L_J$[d]	M_J, %[e]	
1	0	−23	$^6H_{5/2}$	±1/2	74%	28	6343	6348	$^6H_{15/2}$	±11/2	38%
2	145	159	$^6H_{5/2}$	±3/2	67%	29	6561	6572	$^6F_{1/2}$	±1/2	84%
3	247	232	$^6H_{5/2}$	±5/2	72%	30	6699	6705	$^6H_{15/2}$	±3/2	40%
4	1017	998	$^6H_{7/2}$	±3/2	73%	31	6722	6732	$^6F_{3/2}$	±1/2	57%
5	1239	1228	$^6H_{7/2}$	±7/2	30%	32	6751	6782	$^6F_{3/2}$	±3/2	53%
6	1368	1366	$^6H_{7/2}$	±7/2	52%	33	6840	6842	$^6H_{15/2}$	±13/2	15%
7	1412	1412	$^6H_{7/2}$	±5/2	63%	34	6904	6898	$^6H_{15/2}$	±7/2	43%
8	2248	2223	$^6H_{9/2}$	±5/2	57%	35	6940	6946	$^6H_{15/2}$	±9/2	44%
9	2395	2390	$^6H_{9/2}$	±3/2	38%	36	6973	6986	$^6H_{15/2}$	±15/2	44%
10	2461	2449	$^6H_{9/2}$	±9/2	47%	37	7268	7260	$^6F_{5/2}$	±1/2	45%
11	2565	2559	$^6H_{9/2}$	±1/2	33%	38	7378	7361	$^6F_{5/2}$	±3/2	61%
12	2611	2619	$^6H_{9/2}$	±7/2	47%	39	7416	7413	$^6F_{5/2}$	±1/2	41%
13	3550	3548	$^6H_{11/2}$	±5/2	43%	40	8104	8111	$^6F_{7/2}$	±1/2	36%
14	3641	3626	$^6H_{11/2}$	±7/2	58%	41	8115	8132	$^6F_{7/2}$	±5/2	44%
15	3756	3754	$^6H_{11/2}$	±1/2	39%	42	8148	8139	$^6F_{7/2}$	±1/2	45%
16	3820	3821	$^6H_{11/2}$	±1/2	31%	43	8262	8283	$^6F_{7/2}$	±3/2	49%
17	3870	3866	$^6H_{11/2}$	±11/2	31%	44	9264	9265	$^6F_{9/2}$	±5/2	62%
18	3944	3953	$^6H_{11/2}$	±9/2	56%	45	9294	9289	$^6F_{9/2}$	±3/2	43%
19	4864	4868	$^6H_{13/2}$	±1/2	27%	46	9317	9314	$^6F_{9/2}$	±9/2	82%
20	4981	4985	$^6H_{13/2}$	±9/2	36%	47	9361	9356	$^6F_{9/2}$	±7/2	68%
21	5060	5057	$^6H_{13/2}$	±7/2	30%	48	9385	9389	$^6F_{9/2}$	±1/2	50%
22	5175	5179	$^6H_{13/2}$	±3/2	60%	49	10602	10595	$^6F_{11/2}$	±11/2	46%
23	5224	5236	$^6H_{13/2}$	±1/2	46%	50	10623	10614	$^6F_{11/2}$	±9/2	57%
24	5335	5328	$^6H_{13/2}$	±11/2	73%	51	10648	10650	$^6F_{11/2}$	±1/2	53%
25	5367	5379	$^6H_{13/2}$	±13/2	57%	52	10744	10757	$^6F_{11/2}$	±3/2	45%
26	6140	6137	$^6H_{15/2}$	±1/2	47%	53	10768	10781	$^6F_{11/2}$	±5/2	54%
27	6278	6277	$^6H_{15/2}$	±13/2	42%	54	10796	10795	$^6F_{11/2}$	±7/2	43%

[a]Stark level; in D_2 symmetry all Stark levels have the same symmetry label, $^2\Gamma_5$.
[b]Experimental levels taken from Ref. 1.
[c]Calculated levels using parameters from Table III (col. 2) without ccf.
[d]Multiplet of the sextet state in SLJ coupling nomenclature.
[e]Largest percent M_J contribution to the calculated Stark level.

crystal-quantum state is represented only by the combination of M_J states. Examination of column 9 in Table I shows that many of these states are highly mixed with the largest percent M_J contribution being rather small.

Optimization between a final set of 314 calculated-to-observed Stark levels was carried out for a total of 336 predicted Stark levels between 0 and 35 620 cm^{-1}. Spectra observed at higher energy (shorter wavelength) are not sufficiently resolved to merit an analysis. The experimental levels used in the final fitting are designated by a footnote in Table I. By diagonalizing the total energy matrix, we also obtain improved agreement between the experimental and calculated splitting of $^6F_{11/2}$ reported in Ref. 2. This comes about by including all contributions from excited states that were eliminated by the truncation schemes used earlier.[2]

The final set of atomic and crystal-field parameters is given in Table III. Since parameters β, γ, T^n, M_T, and P_T vary little for Sm^{3+} in different host crystals,[16,17] these parameters were held fixed. Atomic parameters F^2, F^4, F^6, α, and ζ varied less than 1.5% from the initial set chosen from the literature.[17] The final set of B_q^k parameters (without ccf) does not change much from the starting set when the analysis is expanded to include the splitting of all 314 Stark levels. As a reference, the starting set of B_q^k obtained from Ref. 2 is listed following the variance associated with the final set of B_q^k parameters obtained in the present study (see column 2, Table III). The rms between the final set of 314 calculated-to-observed Stark levels is 10 cm^{-1}, and is based on five adjustable atomic parameters and nine adjustable one-electron crystal-field parameters. Overall agreement is within the precision of the data and the theoretical expectations for the analysis.

Inclusion of the correlation crystal field in our analysis provides only modest improvement between the calculated and experimental levels, and for that reason the results are not included in Tables I and II. We may point out, however, that the overall splitting of the multiplets $^6H_{5/2}$, $^6H_{7/2}$, $^6H_{11/2}$, $^4P(2)_{5/2}$, $^2K(5)_{13/2}$, and $^2F(5)_{5/2}$ is improved by roughly 10%. However, the rms deviation for all 314 levels is reduced by only 2%, which is not sufficient to merit any conclusions based on ccf interactions. The parameters obtained when ccf is included are given in column 3, Table III.

V. ANALYSIS OF TRANSITION LINE STRENGTHS

The crystal-field parameters reported in Table III (column 2) are used together with a lattice-sum model to determine a

TABLE III. Hamiltonian parameters for Sm^{3+}:YAG.

Parameter[a]	Values excluding corr. crystal field[b] (cm^{-1})	Values including corr. crystal field[c] (cm^{-1})
$\langle E\rangle$	46 977(3)	46 977(3)
F^2	77 619(15)	77 618(15)
F^4	56 297(22)	56 294(22)
F^6	39 856(15)	39 860(15)
α	17.53(0.04)	17.51(0.04)
β	−567	−567
γ	1500	1500
T^2	300	300
T^3	36	36
T^4	56	56
T^6	−347	−347
T^7	373	373
T^8	348	348
ζ_{so}	1167(0.5)	1167(0.5)
M_T	2.60	2.60
P_T	357	357
B_0^2	438(13) [434]	439(13)
B_2^2	107(11) [90]	109(11)
B_0^4	−130(32) [−154]	−118(31)
B_2^4	−1925(13) [−1858]	−1919(18)
B_4^4	−490(23) [−658]	−487(23)
B_0^6	−1589(29) [−1529]	−1575(30)
B_2^6	−687(21) [−712]	−695(20)
B_4^6	945(18) [909]	942(18)
B_6^6	−690(22) [−579]	−689(22)
$G2(4)$		−78.0(63)
$G3(4)$		−4.93(19)
$G10(4)a$		38.9(70)
$G10(4)b$		151(56)

[a]Parameters $\langle E\rangle$ through P_T are described as atomic parameters in the text; parameters B_0^2 through B_6^6 are identified with the crystal field, and parameters $G2(4)$ through $G10(4)b$ are associated with the correlation crystal field.

[b]Final set of values used to calculate the Stark-level energies in Table I (col. 4); values for β through T^8 and M_T and P_T were not varied; the parameter variance is given in parentheses; B_q^k parameters from Ref. 2, representing the starting set in the present study, are given in square brackets; the rms deviation for 314 calculated-to-experimental levels is 10 cm^{-1}.

[c]Final set of values obtained when the correlation crystal field is included in the calculation; only the B_q^k and the ccf parameters were varied with the variance given in parentheses; the rms deviation involving the same levels used in the analysis that did not include ccf terms was reduced by only 2% from the rms given in footnote b.

complete set of even and odd crystal-field components that serve as a starting set of parameters for calculating the transition line strengths. From the model developed by Morrison and Leavitt,[17] we obtain the odd-k crystal-field components $A_{32}=-i1593$, $A_{52}=-i2403$, $A_{54}=i1298$, $A_{72}=i33.6$, $A_{74}=i257$, and $A_{76}=-i208$ all in ($cm^{-1}/Å^k$). The even-k crystal-field components are given by $B_{kq}=\rho_k A_{kq}$, where the radial factors, ρ_k, for Sm^{3+} are given by Morrison and Leavitt.[17]

TABLE IV. Electric-dipole intensity parameters, Sm^{3+}:YAG. Parameters with statistically insignificant values are indicated by parentheses. The starting set was taken from Ref. 25, Table IV, set 1. Since A_{6p}^6 changed less than 1%, we held these values fixed in the final variation analysis.

Parameter (A_{1p}^{λ})	Starting set (10^{-12}) cm	Final set (10^{-12}) cm
A_{20}^2	(22)	83
A_{22}^2	222	121
A_{32}^2	(−106)	−86
A_{32}^4	−216	−120
A_{40}^4	334	154
A_{42}^4	(−37)	(11)
A_{44}^4	20	68
A_{52}^4	−424	−127
A_{54}^4	(−12)	(36)
A_{52}^6	683	652
A_{54}^6	−265	(−0.4)
A_{60}^6	(−11)	(−11)
A_{62}^6	−110	−110
A_{64}^6	(−23)	(−23)
A_{66}^6	143	143
A_{72}^6	(−13)	(−13)
A_{74}^6	(5)	(5)
A_{76}^6	(−73)	(−73)

The transition line strength is expressed as

$$S_{i\to f}=|\langle\Psi_i|\hat{P}|\Psi_f\rangle|^2+|\langle\Psi_i|\hat{M}|\Psi_f\rangle|^2, \tag{5}$$

where $\hat{P}$ is the ''forced'' electric-dipole operator, $\hat{M}$ is the magnetic-dipole operator, and Ψ_i and Ψ_f represent state vectors for the initial and final states in the transition. Since electric-dipole transitions must involve states of opposite parity, such transitions within the $4f^5$ configuration are possible as a result of the crystal-field mixing of opposite-parity states represented by the odd-k terms in the crystal-field Hamiltonian.[23,24]

The line strengths are calculated following methods described by Burdick *et al.*[25] and involve the line-strength parameters, A_{tp}^{λ}, as adjustable parameters. The relationship between these parameters and the parameters obtained from methods developed by Leavitt and Morrison, both in terms of normalization and unit factors, are discussed by Burdick *et al.*[25] in the line-strength analysis of the spectra of Nd^{3+}:YAG. For Sm^{3+} in D_2 sites, there are a possible 5 A_{tp}^2, 11 A_{tp}^4, and 17 A_{tp}^6 adjustable parameters. With the relationship that $(A_{tp}^{\lambda})^*=(-1)^{t+p+1}A_{tp}^{\lambda}$, the number of independent parameters is reduced from 33 to 18 with $3(\lambda=2)$, $6(\lambda=4)$, and $9(\lambda=6)$.

Since Sm^{3+} and Nd^{3+} both occupy similar sites in YAG, reasonable sets of starting A_{tp}^{λ} parameters are available, either from the results of Burdick *et al.*[25] or from the lattice-sum method of Morrison and Leavitt.[17] Beginning with either set, we are able to obtain a final set of parameters listed in Table IV that involves 147 measured-to-calculated line strengths. In the fitting process we found that some of the initial parameters change very little and others become sta-

tistically insignificant. Because the A^6_{6p} parameters change less than 2%, we held these seven parameters fixed. Parameters A^4_{42}, A^4_{54}, and A^6_{54} meet the criteria set by Burdick *et al.*n [25] as being statistically insignificant. These parameters along with the A^6_{6p} parameters that are also statistically insignificant were removed, and the remaining parameters were refit to experiment to generate final line-strength values reported in Table I (column 6). Fitting the line strengths presents problems not encountered in the fitting of the energy levels,[26] but the final set of A^λ_{tp} parameters appearing in Table IV represent the best overall agreement between the measured line strengths chosen and footnoted in Table I. Moreover, the calculated line strengths for transitions not used in the fitting are in general agreement with the measured values to within the limits set by Burdick *et al.*[25,26]

In summary, the present study makes use of both an energy-level analysis and a transition line-strength analysis to interpret the visible and ultraviolet spectra of Sm^{3+}:YAG. The spectra consist of absorption by sextet, quartet, and doublet states that are strongly mixed by the crystal field. An analysis of the calculated-to-experimental energy levels requires diagonalization of the total energy matrix that includes all states of the $4f^5$ electronic configuration. The analysis opens the way for further studies into excited-state absorption and fluorescence lifetimes. Such investigations may encourage further consideration of Sm^{3+}:YAG as a visible laser, at least in the fiber geometry, despite its relatively weak transition line strengths in comparison to those found by Burdick *et al.*[25] for Nd^{3+}:YAG.

ACKNOWLEDGMENTS

One of us (J.B.G.) wishes to express deep appreciation to Dr. M. E. Hills, retired from the Naval Air Warfare Center Weapons Division, China Lake, CA, who from 1986 to 1992 as mentor and colleague participated in the earlier work on Sm^{3+}:YAG.[1,2]

[1] J. B. Gruber, M. E. Hills, M. P. Nadler, M. R. Kokta, and C. A. Morrison, Chem. Phys. **113**, 175 (1987).
[2] S. B. Stevens, C. A. Morrison, M. D. Seltzer, M. E. Hills, and J. B. Gruber, J. Appl. Phys. **70**, 948 (1991).
[3] P. Grünberg, Z. Phys. **225**, 376 (1969).
[4] M. C. Farries, P. R. Morkel, and J. E. Townsend, Electron. Lett. **24**, 709 (1988).
[5] A. A. Kaminskii, *Laser Crystals* (Springer, Berlin, 1981).
[6] B. R. Judd, Phys. Rev. Lett. **39**, 242 (1977).
[7] D. J. Newman, G. G. Siu, and W. Y. P. Fung, J. Phys. C **15**, 3113 (1982).
[8] M. F. Reid, J. Chem. Phys. **87**, 2875 (1987).
[9] J. B. Gruber and M. E. Hills (unpublished) (Naval Air Warfare Center Weapons Division, China Lake, CA, 1990).
[10] M. R. Kokta, Union Carbide Corporation, Electronics Division, Washougal, WA, 1986.
[11] M. Kokta and M. Grasso, J. Solid State Chem. **8**, 357 (1973).
[12] Yu. K. Voronko and A. A. Sobol, Phys. Status Solidi A **27**, 257 (1975).
[13] M. Kokta, J. Solid State Chem. **8**, 39 (1973).
[14] K. Rajnak, R. Mehlhorn, and N. Edelstein, J. Chem. Phys. **58**, 609 (1973).
[15] J. B. Gruber, M. E. Hills, T. H. Allik, C. K. Jayasankar, J. R. Quagliano, and F. S. Richardson, Phys. Rev. B **41**, 7999 (1990).
[16] W. T. Carnall, H. Crosswhite, and H. M. Crosswhite, Argonne National Laboratory Report, U of C-AUA-USERDA, Argonne, IL, 1977 (unpublished).
[17] C. A. Morrison and R. P. Leavitt, in *Handbook on the Physics and Chemistry of the Rare Earths*, edited by K. A. Gschneidner, Jr. and L. Eyring (North-Holland, Amsterdam, 1982), Vol. 5.
[18] C. A. Morrison, *Angular Momentum Theory Applied to Interactions in Solids* (Springer, Berlin, 1988).
[19] B. R. Judd, J. Chem. Phys. **66**, 3163 (1977).
[20] C. L. Li and M. F. Reid, Phys. Rev. B **42**, 1903 (1990).
[21] M. F. Reid and F. S. Richardson, J. Chem. Phys. **79**, 5735 (1983).
[22] M. F. Reid and F. S. Richardson, J. Chem. Phys. **80**, 3579 (1984).
[23] B. R. Judd, Phys. Rev. **127**, 750 (1962).
[24] G. S. Ofelt, J. Chem. Phys. **37**, 511 (1962).
[25] G. W. Burdick, C. K. Jayasankar, F. S. Richardson, and M. F. Reid, Phys. Rev. B **50**, 16 309 (1994).
[26] G. W. Burdick, S. M. Crooks, and M. F. Reid, Phys. Rev. B **59**, 7789 (1999).